Polymer Chemistry

ROYAL SOCIETY OF CHEMISTRY

PAPER

View Article Online
View Journal | View Issue

Cite this: *Polym. Chem.*, 2025, **16**, 1155

Polymethylene with cage silsesquioxane: densely grafted structure prevents side-chain crystallization†

Yu Tomioka,[a] Tomoki Yasui,[a] Kensuke Naka [a,b] and Hiroaki Imoto [*a,b,c]

Received 31st October 2024,
Accepted 28th January 2025

DOI: 10.1039/d4py01222d

rsc.li/polymers

Cage silsesquioxane (POSS, polyhedral oligomeric silsesquioxane) is a crucial building block in the development of organic–inorganic hybrid polymers. However, polymers incorporating POSS units in their side chains often exhibit poor film-forming properties because of the high crystallinity of POSS. In this study, polymethylene densely grafted with POSS units was synthesized. This POSS-polymethylene structure produced a homogeneous, transparent cast film, in contrast to the turbid film formed by POSS-polyacrylate. The significant difference in the film quality was attributed to the inhibition of POSS crystallization, facilitated by the dense tethering of POSS on the polymethylene backbone.

Introduction

The integration of inorganic elements into organic polymers is a significant strategy for achieving enhanced performance and functionality, which are often unattainable using commodity polymers.[1,2] Siloxane, which is particularly valued for its stability, transparency, structural diversity, and modifiability, is a prime candidate for this purpose.[3] A notable siloxane variant, polyhedral oligomeric silsesquioxane (POSS), is well-suited for creating polymerizable molecular structures.[4] POSS has been incorporated into polymers at various points, including the main chain,[5] side chain,[6] cross-linking sites,[7] and terminal ends.[8] Among these, side-chain polymers are essential for achieving high-POSS-content polymers. The synthesis of side-chain monomers is relatively simple because mono-functional POSS derivatives can be easily obtained from commercially available sources.[9] However, homopolymers containing POSS in each repeating unit are rare (Fig. 1a).[10] The high crystallinity of POSS often leads to the aggregation of high-POSS content polymers, producing turbid and brittle films.[10a]

To address the challenges posed by the crystallinity, we focused on the development of amorphous POSS homopolymers.[10a,11] For instance, by incorporating partially hydrolyzed cage structures, the crystallinity of homopolymers can be reduced as the cages disrupt the symmetry of the POSS units, allowing for the formation of amorphous, optically transparent films (Fig. 1b).[11a–c] However, the selective synthesis of open-cage POSS monomers remains highly dependent on the substituents attached to POSS. Therefore, a versatile and simple strategy for inhibiting POSS crystallization is highly desired.

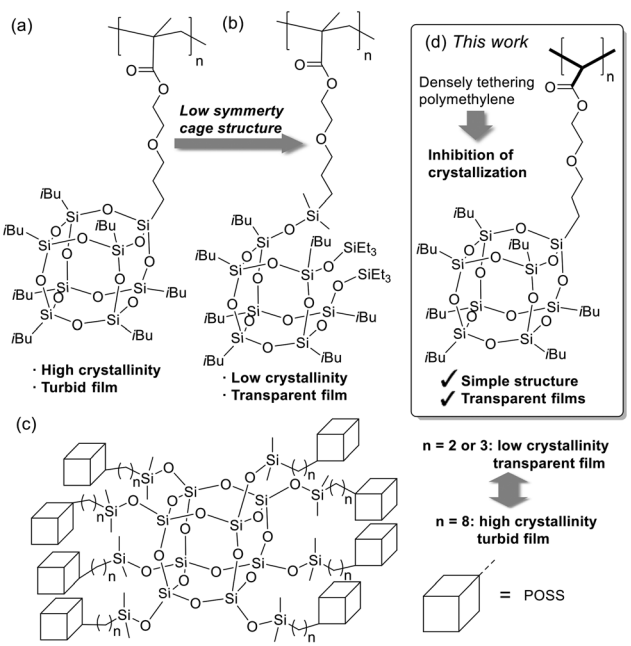

Fig. 1 (a) Cubic and (b) open-cage POSS polymers. (c) POSS dendrimers on OS core. (d) POSS polymethylene (this work).

[a]*Faculty of Molecular Chemistry and Engineering, Kyoto Institute of Technology, Goshokaido-cho, Matsugasaki, Sakyo-ku, Kyoto 606-0962, Japan. E-mail: himoto@kit.ac.jp*
[b]*Materials Innovation Lab, Kyoto Institute of Technology, Goshokaido-cho, Matsugasaki, Sakyo-ku, Kyoto 606-0962, Japan*
[c]*FOREST, JST, Honcho 4-1-8, Kawaguchi, Saitama 332-0012, Japan*

†Electronic supplementary information (ESI) available: NMR, MALDI-TOFMS, and SEC. See DOI: https://doi.org/10.1039/d4py01222d

In a previous study, we investigated a dendritic POSS octamer in which eight POSS units were grafted onto an octasilicate (OS) core (Fig. 1c).[12] Shorter linkers between the POSS units and the OS core produced transparent films, whereas longer linkers promoted POSS crystallization.[12a] This result suggests that densely substituted POSS units can prevent the formation of a crystalline structure, a concept that we extended to POSS-tethered polymers.

Polymethylene serves as an excellent platform for densely aligning functional units in polymer side chains.[13] Unlike the POSS side chains in polymethacrylate, which tend to aggregate, the densely aligned structure of POSS in polymethylene is expected to inhibit crystallization. For polymethylene synthesis, Pd-catalyzed denitrogenative polymerization of diazoacetate monomers is highly effective.[13] In this process, Pd–Ph species, formed *via* transmetalation from tetraphenylborate (BPh_4^-), initiate polymerization. During propagation, the Pd center reacts with the diazoacetate monomer, generating a Pd–carbene intermediate through denitrogenation, followed by migratory insertion of the carbene carbon into the Pd–Ph bond. Ihara *et al.* created polymethylenes with bulky side chains, such as cyclotriphosphazenes and poly(benzyl ether) dendrons, through the Pd-catalyzed denitrogenative polymerization of diazoacetate monomers.[14] Importantly, compared to less sterically hindered side chains, bulky side chains can suppress undesirable side reactions, enabling well-controlled polymerization. This polymerization method is particularly advantageous for synthesizing POSS-tethered polymethylenes because of the bulkiness of the POSS units.

In this study, we design a novel POSS-diazoacetate monomer, where the Pd-catalyzed denitrogenative polymerization yields a well-controlled POSS-tethering polymethylene. As expected, the resulting polymer forms a transparent film, whereas the polyacrylate variant undergoes aggregation and produces a turbid film. X-ray diffraction (XRD) analysis provides insights into the assembly structures of the POSS units in polymethylene and polyacrylate.

Results and discussion

The syntheses of the POSS-diazoacetate and POSS-acrylate monomers (**3** and **4**, respectively) are outlined in Scheme 1. The procedures for synthesizing **3** [15] and **4** [10a] were adapted from previous reports. Heptaisobutyl-POSS alcohol **1** was prepared according to a previously described procedure.[10a] Condensation of **1** with bromoacetyl bromide yielded POSS-bromoacetate **2**, which was subsequently reacted with *N*,*N*′-bis(*p*-toluenesulfonyl)hydrazine to produce POSS-diazoacetate monomer **3**. Similarly, the condensation of **1** with acryloyl chloride afforded POSS-acrylate monomer **4**. The structures and purities of the synthesized compounds were confirmed using a combination of NMR spectroscopy, MALDI-TOF MS, elemental analysis, Fourier transform infrared (FT-IR) spectroscopy, and size exclusion chromatography (SEC).

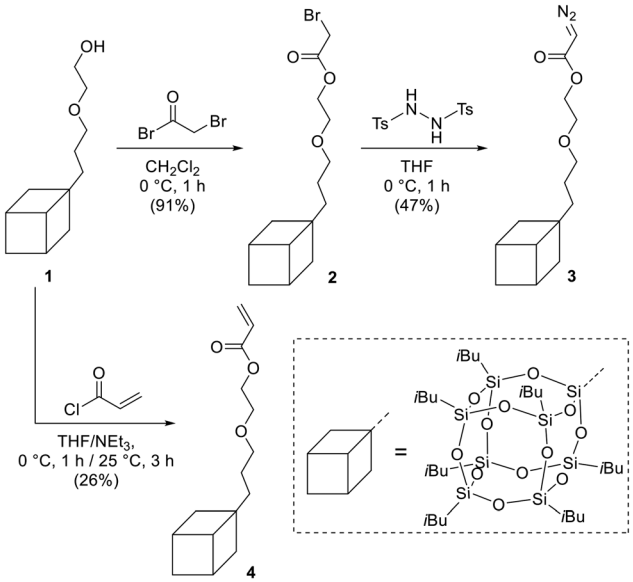

Scheme 1 Syntheses of POSS monomers **3** and **4**. Cube indicates heptaisobutyl-substituted POSS unit.

The reaction conditions for the synthesis of POSS-tethered polymethylene **P1** were optimized (Table 1). The number-average molecular weight (M_n) and weight-average molecular weight (M_w) were estimated by SEC using polystyrene standards. Polymerization was initially conducted in tetrahydrofuran (THF) using allylpalladium(II) chloride (π-allylPdCl) as the catalyst, albeit with a low conversion of only 15% (entry 1). Inspired by the work of Ihara and Shimomoto,[16] we introduced sodium tetraphenylborate ($NaBPh_4$) as a co-catalyst (entry 2), which significantly improved both the molecular weight (M_n = 8100) and conversion (73%), with a low dispersity index (M_w/M_n = 1.11). This narrow dispersity suggests that the bulky side chains of POSS effectively suppress the side reactions.

Further variations in the reaction temperature, such as lowering it to −15 °C or raising it to 50 °C (entries 3 and 4), resulted in slight decreases in the molecular weight and conversion. Adjusting the ratio of the monomer to the Pd catalyst ([**3**]/[Pd]) (entries 5–7) and changing the monomer concentration (entry 8) did not significantly enhance the M_n (up to 7500) or conversion (up to 70%). The lack of significant improvement with increased [**3**]/[Pd] ratios might be attributed to chain transfer reactions, as suggested by Ihara and Shimomoto in similar polymerization systems.[17] Therefore, the optimal conditions were identified, as described in entry 2.

Polymer **P1** was synthesized under these optimized conditions and purified by preparative HPLC to remove the low-molecular-weight components (Scheme 2a). During purification, the dimer **D1** was isolated as a mixture of *cis* and *trans* isomers (*cis*/*trans* = 21/79), as identified by NMR spectroscopy and MALDI-TOF MS. This dimer likely formed through C=C bond formation between diazo-bearing carbons of the monomers during polymerization, as previously reported in similar systems.[14b,17] Polymer **P2**, the POSS-tethered polyacrylate, was

Table 1 Optimization of Pd-catalyzed denitrogenative polymerization of monomer **3**

Entry	Catalyst	Temp. [°C]	[3]/[Pd][a]	[3] [mM]	M_n[b]	M_w/M_n[b]	Conversion[b] [%]
1	π-AllylPdCl	25	50	200	5400	1.09	15
2	π-AllylPdCl/$NaBPh_4$	25	50	200	8100	1.11	73
3	π-AllylPdCl/$NaBPh_4$	−15	50	200	7700	1.11	70
4	π-AllylPdCl/$NaBPh_4$	50	50	200	7500	1.10	66
5	π-AllylPdCl/$NaBPh_4$	25	30	200	6700	1.09	66
6	π-AllylPdCl/$NaBPh_4$	25	100	200	7100	1.14	52
7	π-AllylPdCl/$NaBPh_4$	25	200	200	7100	1.14	42
8	π-AllylPdCl/$NaBPh_4$	25	50	500	7500	1.11	70

[a] Molar ratio of monomer **3** and Pd catalyst. [b] Estimated by SEC with polystyrene standards (THF, 1 mL min^{-1}).

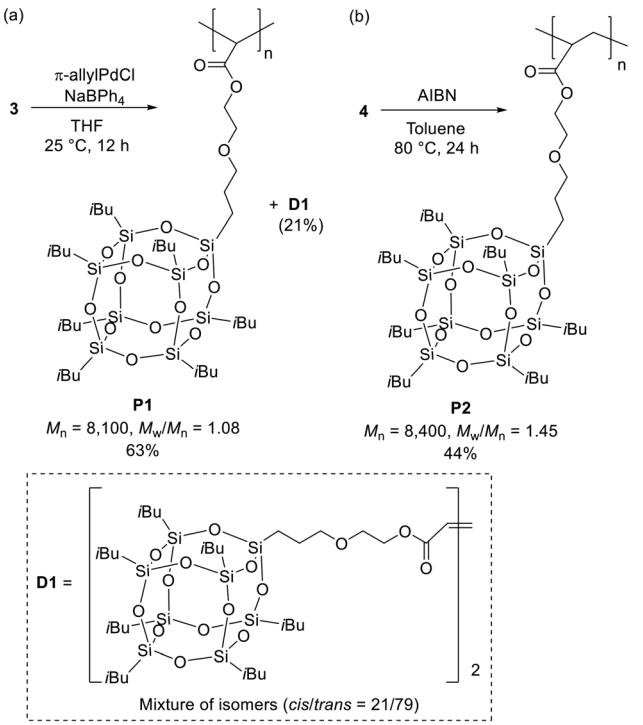

Scheme 2 Syntheses of (a) polymer **P1** and dimer **D1**, and (b) polymer **P2**.

synthesized *via* free-radical polymerization using 2,2′-azobis (isobutyronitrile) (AIBN) as the initiator, following a reported procedure for POSS-tethered polymethacrylates (Scheme 2b).[10a] While monomer conversion was relatively high (81%), the isolated yield was reduced to 44% due to the purification process involving preparative HPLC (Fig. S27†). SEC analysis confirmed that the molecular weights of **P1** (M_n = 8100) and **P2** (M_n = 8400) were similar, although **P2** exhibited higher dispersity (M_w/M_n = 1.45) than **P1** (M_w/M_n = 1.08), likely because of the nature of free-radical polymerization in **P2**.

In the ^{1}H-NMR spectra, the signals corresponding to the isobutyl groups (δ = 1.86 (methyne), 0.95 (methyl), 0.59 (methylene) ppm) in **P1** (Fig. S10†) were notably broader than those in **P2** (Fig. S18†), indicating that the molecular mobility of the POSS units in **P1** was more restricted. Additionally, the ^{1}H-NMR spectrum of **P1** exhibited a broad signal corresponding to the methylene units in the main chain around 3.4–2.8 ppm. The assignment of this signal was supported by the ^{1}H–^{13}C HSQC NMR spectrum (Fig. S13†). Ihara and Shimomoto previously reported that polymerization catalyzed by π-allylPdCl results in atactic polymethylene, with broad methylene signals around 3 ppm.[18] Therefore, it was reasonable to conclude that **P1** had an atactic structure. The weak and broad signal around 7.2 ppm in the ^{1}H NMR spectrum, corresponding to the terminal group of **P1**, was insufficiently resolved to determine the M_n value from integral ratios.

Chloroform ($CHCl_3$) solutions of polymers **P1** and **P2** (75 g L^{-1}) were cast onto glass substrates and dried under ambient conditions (25 °C, 1 atm) for 24 h. The cast film of **P1** was transparent, whereas that of **P2** appeared turbid (Fig. 2a). Even after annealing at around the melting points for 24 h, the film appearances remained unchanged (Fig. S31†). This suggests that the dense tethering structure of the polymethylene backbone in **P1** effectively inhibited the aggregation of the POSS units. In contrast, the polyacrylate backbone of **P2** allowed for greater molecular mobility, promoting the crystallization of POSS. The scanning electron microscopy (SEM) images of **P1** and **P2** revealed no micrometer-scale surface roughness (which can cause light scattering), although cracks were present. This indicates that the aggregates in **P2** were likely at the submicron scale, contributing to visible-light scattering and resulting in turbidity. The transmittance spectra (Fig. 2b) confirmed that

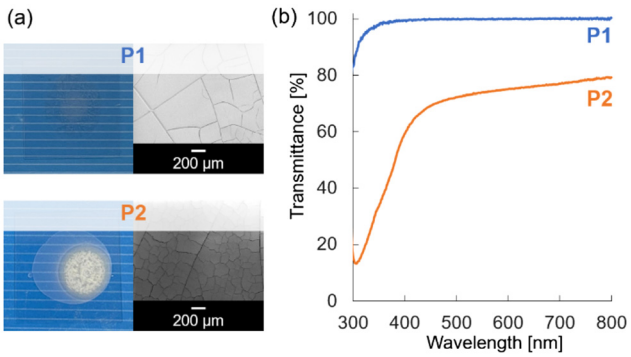

Fig. 2 (a) Photographs (left) and SEM images (right) of **P1** and **P2**. (b) Transmittance spectra of **P1** and **P2**.

P1 exhibited significantly higher transparency than **P2** in the visible-light range (350–800 nm).

Thermogravimetric analysis (TGA) and differential scanning calorimetry (DSC) were used to evaluate the thermal properties of **P1**, **P2**, and monomeric POSS **1** (Fig. 3 and Table 2). The TGA results showed that the decomposition temperatures at 5 wt% loss (T_{d5}) were 299 °C (**P1**), 340 °C (**P2**), and 239 °C (**1**) (Fig. 3a). Polymerization enhanced the thermal stability of both **P1** and **P2** compared to that of monomeric POSS **1**. The higher thermal stability of **P2** compared to that of **P1** is likely due to aggregation of the POSS units, which is more pronounced in polyacrylate-based structures. Generally, polyacrylates exhibit better thermal stability than polymethylenes.[19]

DSC measurements (Fig. 3b) revealed that the melting points (T_m) of **P1**, **P2**, and **1** were 122, 162, and 170 °C, respectively. The melting peaks of **P1** and **P2** were reproducible across three heating–cooling cycles. During the cooling process, a clear crystallization peak was observed for **P2** (Fig. S30†). The data indicate that the crystalline domains in **P2** were significantly larger than those in **P1** and comparable to those in **1**. The estimated melting enthalpy (ΔH) of **P1** (1.2 J g^{-1}) was much lower than that of **P2** (17.9 J g^{-1}), suggesting that the crystallinity of POSS in **P1** was greatly reduced by the polymethylene backbone. Furthermore, the smaller estimated melting entropy (ΔS) of **P1** (3.1 mJ K^{-1} g^{-1}) compared that of **P2** (40.9 mJ K^{-1} g^{-1}) supports the postulate that the molecular mobility of the POSS units in **P1** was more restricted. The ΔH and ΔS values for **1** (19.8 J g^{-1} and 44.6 mJ K^{-1} g^{-1}, respectively) were similar to those of **P2**, indicating that the POSS units in **P2** were able to crystallize, similarly to monomeric POSS, due to the higher molecular mobility afforded by the polyacrylate backbone.

XRD analysis was performed to further investigate the aggregation structures of the POSS units in **P1**, **P2**, and **1** (Fig. 4a). The peak positions in the XRD patterns of **P1** and **P2** corresponded well with those of **1**, indicating that the signals are associated with aggregation of the POSS units. However, the XRD peak of **P1** was much broader than that of **P2**, reflecting the lower crystallinity of the POSS units in **P1**. This difference explains why **P1** formed a transparent film, whereas **P2** produced a turbid film.

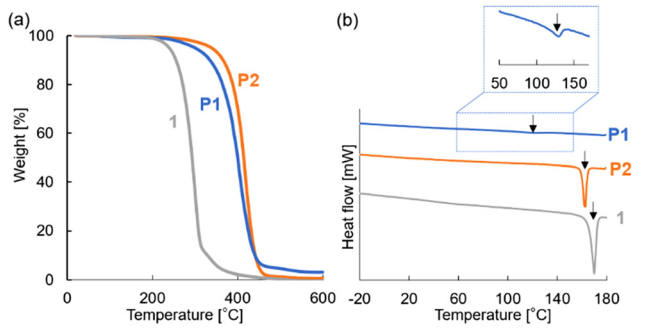

Fig. 3 (a) TGA thermograms and (b) DSC curves (second scan) of **P1**, **P2**, and **1** (under N_2, 10 °C min^{-1}). Arrows indicate the melting points.

Table 2 Thermal properties of **P1**, **P2**, and **1**

	T_{d5}[a] [°C]	T_m[b] [°C]	ΔH[b] [J g^{-1}]	ΔS[b] [mJ K^{-1} g^{-1}]
P1	299	122	1.2	3.1
P2	340	162	17.9	40.9
1	239	170	19.8	44.6

[a] Estimated by TGA. [b] Estimated by DSC. T_{d5} = decomposition temperature corresponding to 5 wt% loss, T_m = melting point, ΔH = melting enthalpy, and ΔS = melting entropy.

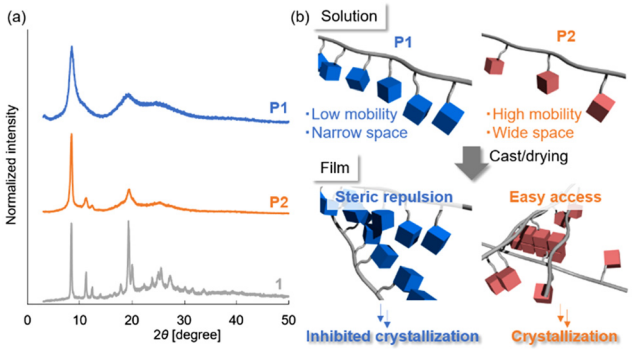

Fig. 4 (a) XRD patterns of **P1**, **P2**, and **1**. (b) Schematic of plausible mechanism for differences in the crystallization behaviors of **P1** and **P2**.

A plausible mechanism for the inhibition of POSS crystallization in **P1** is shown in Fig. 4b. The tightly packed structure of the POSS units along the polymethylene backbone in **P1** prevents crystallization during film formation. Additionally, the densely tethered POSS units provide insufficient space for crystallization along the polymethylene chains. In contrast, the POSS units in **P2**, which have a polyacrylate backbone, have higher molecular mobility and sufficient space to form crystallized structures.

Conclusions

Polymethylene **P1** was successfully synthesized to achieve dense alignment of the POSS units in the side chain. The Pd-catalyzed denitrogenative polymerization of POSS-diazoacetate monomer **3** was well controlled, with the bulky POSS units ensuring low dispersity index in **P1**. The cast film of **P1** was transparent and homogeneous, in stark contrast to its polyacrylate counterpart, **P2**, which formed aggregates, resulting in a turbid film. DSC and XRD analyses revealed that the crystallization of the POSS units in **P1** was effectively suppressed by the densely tethered polymethylene backbone. This study demonstrated a novel molecular design approach for the development of side-chain POSS polymers with excellent film-forming properties. Further studies on a range of POSS polymethylenes are ongoing, and the results will be reported in future publications.

Experimental

Materials

Potassium carbonate (K_2CO_3), dichloromethane (CH_2Cl_2), sodium chloride (NaCl), 1,8-diazabicyclo[5.4.0]-7-undecene (DBU), chloroform ($CHCl_3$), ethyl acetate (EtOAc), triethylamine (Et_3N), acetonitrile (MeCN), hydrochloric acid (35%), α,α′-azobisisobutyronitrile (AIBN), and tetrahydrofuran (THF, HPLC grade) were purchased from Nacalai Tesque (Kyoto, Japan). CH_2Cl_2 (super dehydrated grade), distilled water, anhydrous magnesium sulfate ($MgSO_4$), sodium hydrogen carbonate ($NaHCO_3$), *n*-hexane, toluene (super dehydrated grade), and $CDCl_3$ (D = 99.8%) were purchased from FUJIFILM Wako Pure Chemical Co. (Osaka, Japan). Bromoacetyl bromide, acryloyl chloride, and sodium tetraphenylborate ($NaBPh_4$) were purchased from Tokyo Chemical Industry (Tokyo, Japan). Superdehydrated THF (super dehydrated grade) was purchased from Kanto Chemical Co., Inc. (Tokyo, Japan). Allylpalladium (II) chloride dimer ([π-allylPdCl]$_2$) was purchased from Sigma-Aldrich (Hattiesburg, MS). Heptaisobutyl-hydroxyethoxypropyl CC-POSS (**1**)[10a] and *N*,*N*′-ditosylhydrazine[15] were prepared according to literature procedures. The starting material for **1** (heptaisobutyl trisilanol POSS) was purchased from Hybrid Plastics Inc. (Hattiesburs, MS).

Measurements

^{1}H (400 MHz), ^{13}C (100 MHz), and ^{29}Si (80 MHz) nuclear magnetic resonance (NMR) spectra were recorded at 25 °C on a Bruker AVANCE III 400 NMR spectrometer (Bruker BioSpin GmbH, Rheinstetten, Germany) in $CDCl_3$. The following abbreviations are used: s, singlet; d, doublet; t, triplet; q, quartet; m, multiplet; br, broad. The NMR measurements were performed with a sample concentration of about 30 mg in 0.4 mL of solvent. The polymer's ^{13}C-NMR spectra were collected following 12 hours of signal accumulation. The 2D NMR (HSQC and HMBC) spectra were recorded at 25 °C on a Bruker AVANCE III 500 NMR spectrometer (Bruker BioSpin GmbH, Rheinstetten, Germany) in $CDCl_3$. Matrix-assisted laser desorption ionization time-of-flight mass spectrometry (MALDI-TOF-MS) data were recorded on a JMS-S3000 instrument (JEOL Ltd, Tokyo, Japan) using *trans*-2-[3-(4-*tert*-butylphenyl)-2-methyl-2-propenylidene]malononitrile (DCTB) as the matrix (20 mg mL^{-1} in $CHCl_3$) and sodium trifluoroacetate as a cationizing agent (1 mg mL^{-1} in THF). The molecular weights were determined by size exclusion chromatography (SEC) using an LC-6AD column (Shimadzu, Kyoto, Japan) equipped with a Shodex KF-805L column (Showa Denko, Tokyo, Japan) and an RI detector RID-20A (Shimadzu). Preparative high-performance liquid chromatography (HPLC) for purification was performed on an LC-6AD (Shimadzu) instrument with a Shodex KF-2003 (Showa Denko) tandem column system using $CHCl_3$ as the eluent (4.0 mL min^{-1}). Thermogravimetric analysis (TGA) and differential scanning calorimetry (DSC) measurements were performed by using Shimadzu DTG-60 and DSC-60 Plus (Shimadzu) instruments, respectively, under N_2 atmosphere, at heating rate of 10 °C min^{-1}. Transmittance spectra were recorded using a JASCO spectrophotometer (V-670 KNN, JASCO). X-ray diffractometry (XRD) studies were performed on a Rigaku MiniFlex600-C X-ray diffractometer with Cu-Kα radiation (λ = 1.5406 Å) in the $2\theta/\theta$ mode at room temperature. The 2θ scan data were collected at 0.01° intervals; the scan speed was 10° (2θ) min^{-1}. Scanning electron microscopy (SEM) images of the films were obtained using a VE-8800 system (KEYENCE, Osaka, Japan). Elemental analyses were performed on a YANAKO CHN Corder MT-5. Fourier transform infrared (FT-IR) spectra were obtained using a JASCO FT/IR-4600 spectrometer (JASCO).

Synthesis procedure and characterization data

POSS-bromoacetate (2). A CH_2Cl_2 solution (19 mL) of **1** (3.49 g, 3.80 mmol) and K_2CO_3 (2.62 g, 19.0 mmol) was cooled at 0 °C under N_2 atmosphere, and bromoacetyl bromide (0.99 mL, 11.4 mmol) was slowly added. After stirring for 1 h at 0 °C, the reaction was quenched with H_2O. The solution was extracted three times with CH_2Cl_2. The organic phase was washed with brine and dried over $MgSO_4$. The solvent was evaporated and the residue (3.59 g, 3.45 mmol, 91%) was used in the next reaction without purification because of its high purity. ^{1}H-NMR (in $CDCl_3$, 400 MHz): δ (ppm): 4.33–4.31 (m, 2H), 3.87 (s, 2H), 3.66–3.63 (m, 2H), 3.44 (t, J = 7.0 Hz, 2H), 1.92–1.78 (m, 7H), 1.72–1.64 (m, 2H), 0.95(d, J = 6.4 Hz, 42H), 0.61–0.59 (m, 16H). ^{13}C-NMR (in $CDCl_3$, 100 MHz): δ (ppm):167.3, 73.5, 68.0, 65.4, 25.7, 23.9, 23.8, 22.7, 22.5, 8.2. ^{29}Si-NMR (in $CDCl_3$, 80 MHz): δ (ppm): −67.4, −67.7, −67.9. MALDI-TOF-MS (*m*/*z*. [M + Na]$^+$): 1061.2341, (calc.); 1061.2353 (observed). Anal. calcd for $C_{35}H_{75}BrO_{15}Si_8$: C, 40.40; H, 7.27. Found: C, 40.43; H, 7.37.

POSS-diazoacetate monomer (3). A THF solution (16 mL) of **2** (3.36 g, 3.23 mmol) and *N*,*N*′-ditosylhydrazine (2.20 g, 6.46 mmol) was cooled to 0 °C under N_2 atmosphere, and DBU (2.41 mL, 16.1 mmol) was added dropwise. After stirring at 0 °C for 1 h, the reaction was quenched with saturated $NaHCO_3$aq. The solution was extracted three times with $CHCl_3$. The organic phase was washed with brine, dried over $MgSO_4$, and evaporated to obtain the crude product. Purification by silica gel chromatography (*n*-hexane/EtOAc = 15 : 1) afforded **3** as a pale yellow powder (1.48 g, 1.50 mmol, 47%). ^{1}H-NMR (in $CDCl_3$, 400 MHz): δ (ppm): 4.79 (s, 1H), 4.32–4.29 (m, 2H), 3.64–3.61 (m, 2H), 3.43 (t, J = 7.0 Hz, 2H), 1.92–1.78 (m, 7H), 1.72–1.64 (m, 2H), 0.95 (d, J = 6.8 Hz, 42H), 0.62–0.57 (m, 16H). ^{13}C-NMR (in $CDCl_3$, 100 MHz): δ (ppm): 167.0, 73.6, 68.6, 64.2, 46.4, 25.8, 24.0, 22.9, 22.6, 8.3. ^{29}Si-NMR (in $CDCl_3$, 80 MHz): δ (ppm): −67.4, −67.7, −67.9. MALDI-TOF-MS (*m*/*z*. [M + Na]$^+$): 1009.3141, (calc.); 1009.3028 (observed). Anal. calcd for $C_{35}H_{74}N_2O_{15}Si_8$: C, 42.56; H, 7.55; N, 2.84. Found: C, 42.36; H, 7.74; N, 2.48.

POSS-acrylate monomer (4). A THF solution (30 mL) of **1** (3.00 g, 3.26 mmol) and Et_3N (2.75 mL, 19.9 mmol) was cooled to 0 °C under N_2 atmosphere. Acryloyl chloride (1.60 ml, 19.9 mmol) was then added dropwise. The reaction mixture was stirred at 0 °C for 1 h and warmed to room temperature under N_2 atmosphere. After the reaction, the volatiles were removed *in vacuo* and the residue was extracted using

n-hexane. After removing the solvents *in vacuo*, the residue was washed with MeCN to obtain **4** as a pale yellow powder (0.836 g, 0.859 mmol, 26%). ^{1}H-NMR (in $CDCl_3$, 400 MHz): δ (ppm): 6.43 (dd, J = 17 Hz, 1.4 Hz, 1H), 6.16 (dd, J = 17 Hz, 10 Hz, 1H), 5.83 (dd, J = 10 Hz, 1.6 Hz, 1H), 4.32–4.29 (m. 2H), 3.67–3.65 (m, 2H), 3.45 (t, J = 7.0 Hz, 2H), 1.90–1.80 (m, 7H), 1.72–1.65 (m, 2H), 0.95 (d, J = 6.8 Hz, 42H), 0.61–0.59 (m, 16H). ^{13}C-NMR (in $CDCl_3$, 100 MHz): δ (ppm): 166.3, 131.0, 128.5, 73.6, 68.5, 63.9, 25.8, 24.0, 22.9, 22.7, 8.3. ^{29}Si-NMR (in $CDCl_3$, 80 MHz): δ (ppm): −67.4, −67.7, −67.9. MALDI-TOF-MS (m/z. $[M + Na]^+$): 995.3236, (calc.); 995.3218 (observed). Anal. calcd for $C_{36}H_{76}O_{15}Si_8$ (+0.5% water): C, 44.19; H, 7.89. Found: C, 43.81; H, 7.70.

POSS-polymethylene (P1) and dimer (D1). A THF (0.2 mL) solution of [π-allylPdCl]$_2$ (0.741 mg, 2.02 μmol) was cooled to −78 °C under N_2 atmosphere and added to $NaBPh_4$ (2.08 mg, 6.07 μmol). The resulting mixture was stirred at −78 °C for 10 min. A THF solution (0.3 mL) of **3** (100 mg, 0.101 mmol) was added dropwise at −78 °C, after which the reaction mixture was warmed to 25 °C and stirred for 12 h. The volatiles were removed *in vacuo*, and 1 N HCl(aq.) and $CHCl_3$ were added to the residue. The aqueous phase was extracted with $CHCl_3$, and the organic phase was dried over $MgSO_4$. The solvent was evaporated and the residue was purified by preparative HPLC to obtain **P1** (61.1 mg, 63%) and **D1** (20.6 mg, 21%). **D1** was isolated as a mixture of isomers (*cis*/*trans* = 21/79). **P1**: ^{1}H-NMR (in $CDCl_3$, 400 MHz): δ (ppm): 4.10 (br, 2H), 3.57 (br, 2H), 3.37 (br, 2H), 3.07 (br, 1H), 1.86 (br, 7H), 1.62 (br, 2H), 0.95 (d, J = 6.4 Hz, 42H), 0.59 (br, 16H). ^{13}C-NMR (in $CDCl_3$, 100 MHz): δ (ppm): 169.8, 74.0, 67.6, 63.4, 26.0, 24.0, 23.2, 22.7, 45.8, 8.5. ^{29}Si-NMR (in $CDCl_3$, 80 MHz): δ (ppm): −67.4, −67.7, −68.0. **D1**: ^{1}H-NMR (in $CDCl_3$, 400 MHz): δ (ppm): 6.92 (s, *trans*), 6.28 (s, *cis*), 4.35–4.32 (m, 4H), 3.67–3.64 (m, 4H), 3.46–3.41 (m, 4H), 1.90–1.79 (m, 14H), 1.72–1.65 (m, 4H), 0.95 (d, J = 6.4 Hz, 84H), 0.61–0.59 (m, 32H). ^{13}C-NMR (in $CDCl_3$, 125 MHz): δ (ppm): 165.3 (*cis*), 165.0 (*trans*), 133.8 (*trans*), 130.1 (*cis*), 73.7 (*trans*), 73.7 (*cis*), 68.3 (*trans*), 68.2 (*cis*), 64.7 (*trans*), 64.6 (*cis*), 25.8, 24.0, 22.9, 22.6, 8.3. ^{29}Si-NMR (in $CDCl_3$, 80 MHz): δ (ppm): −67.4, −67.7, −67.9. MALDI-TOF-MS (m/z. $[M + Na]^+$): 1939.6261, (calc.); 1939.6221 (observed).

POSS-polyacrylate (P2). A toluene solution (0.3 mL) of **4** (300 mg, 0.308 mmol) and AIBN (5.06 mg, 30.8 μmol) was stirred at 80 °C for 24 h under N_2 atmosphere. After the reaction, the volatiles were removed *in vacuo*. The residue was purified using preparative HPLC to obtain **P2** (133 mg, 44%). ^{1}H-NMR (in $CDCl_3$, 400 MHz): δ (ppm): 4.16 (br, 2H), 3.57 (br, 2H), 3.40 (br, 2H), 2.33 (br, 3H), 1.90–1.80 (m, 7H), 1.65 (br, 2H), 0.95 (d, J = 6.4 Hz, 42H), 1.18 (d, J = 6.8 Hz, 16H). ^{13}C-NMR (in $CDCl_3$, 100 MHz): δ (ppm): 174.5, 73.6, 68.1, 63.5, 41.5, 31.4, 25.9, 24.0, 22.9, 22.7, 8.4. ^{29}Si-NMR (in $CDCl_3$, 80 MHz): δ (ppm): −67.4, −67.7, −67.9.

Film fabrication

A $CHCl_3$ solution (0.20 mL) of the polymer (15 mg) was prepared. The solution was cast onto a glass substrate and dried at 25 °C for 24 h.

Author contributions

Y. Tomioka: synthesis, structural analysis, data curation, writing – original draft; T. Yasui: structural analysis, data curation, writing – original draft; K. Naka: conceptualization, investigation, writing – review and editing, supervision; H. Imoto: conceptualization, investigation, writing – original draft, writing – review and editing, funding acquisition project administration, supervision.

Data availability

The authors confirm that the data supporting the findings of this study are available within the article and its ESI.†

Conflicts of interest

There are no conflicts to declare.

Acknowledgements

We appreciate Prof. Hiroaki Shimomoto (Ehime University) for the constructive discussion on the synthesis and structural analysis of polymethylene.

References

1 (*a*) *Main Group Strategies towards Functional Hybrid Materials*, ed. T. Baumgartner and F. Jaekle, Wiley, 2018; (*b*) *New Polymeric Materials Based on Element-Blocks*, ed. Y. Chujo, Springer, Singapore, 2019.

2 (*a*) J. Bedard and S. Chitnis, *Chem. Mater.*, 2023, **35**, 8338–8352; (*b*) F. Vidal and F. Jäkle, *Angew. Chem., Int. Ed.*, 2019, **58**, 5846–5870; (*c*) M. Gon, K. Tanaka and Y. Chujo, *Polym. J.*, 2018, **50**, 109–126; (*d*) M. Gon, K. Tanaka and Y. Chujo, *Bull. Chem. Soc. Jpn.*, 2017, **90**, 463–474.

3 *Silicones and Silicone-Modified Materials*, ed. S. J. Clarson, J. J. Fitzgerald, M. J. Owen and S. D. Smith, ACS Symposium Series, 2000, vol. 729.

4 For reviews, see: (*a*) F. Chen, F. Lin, Q. Zhang, R. Cai, Y. Wu and X. Ma, *Macromol. Rapid Commun.*, 2019, **40**, 1900101; (*b*) H. Shi, J. Yang, M. You, Z. Li and C. He, *ACS Mater. Lett.*, 2020, **2**, 296–316; (*c*) C. Wang, L. Zhou, Q. Du, T. Shan, K. Zheng, J. He, H. He, S. Chen and X. Wang, *Polym. Int.*, 2022, **71**, 379–392; (*d*) Y. Liu, X.-Y. Yan, Q.-Y. Guo, H. Lei, X. Liu, X. Li, Y. Wu, W. Zhang, G. X. Liu and S. Z. D. Cheng, *Macromol. Chem. Phys. Commun.*, 2023, **224**, 2200357; (*e*) L. Miao, L. Zhan, S. Liao, Y. Li, T. He, S. Yin, L. Wu and H. Qiu, *Macromol. Rapid Commun.*, 2024, **45**, 2300601; (*f*) L. Li, H. Wang and S. Zheng, *J. Polym. Sci.*, 2024, **64**, 583–613.

5 Recent papers, see: (*a*) H. Wang, L. Li, T. Zhang and S. Zheng, *Eur. Polym. J.*, 2024, **202**, 112652; (*b*) H. Wang,

G. Hang, J. Hu, Y. Gao, L. Li and S. Zheng, *ACS Appl. Polym. Mater.*, 2023, **5**, 4274–4287; (*c*) T. Kamitani, M. Nakamura, S. Watase, T. Suzuki, H. Imoto and K. Naka, *ACS Appl. Polym. Mater.*, 2023, **5**, 5169–5176; (*d*) H. Chi, M. Wang, J. Li, H. Tian, Y. T. Chong, S. H. Lim, Y. Wang and F. Wang, *ACS Appl. Polym. Mater.*, 2022, **4**, 5882–5890; (*e*) J. Guan, Z. Zhang and R. M. Laine, *Macromolecules*, 2022, **55**, 5403–5411.

6 Recent papers, see: (*a*) F. Feng, S. Zhang, W. Wang, C. Hong, M. Zhang, F. Yang, Y. Peng, F. Jia and H. Liu, *Giant*, 2024, **19**, 100304; (*b*) A. R. Uribe, *Polymer*, 2023, **275**, 125933; (*c*) S. Iwao, N. Kurono, W. Higashiguchi, T. Hayakawa, N. Ohta, K. Kamitani, S. Fujii, Y. Nakamura and T. Hirai, *Chem. Lett.*, 2022, **51**, 781–783; (*d*) A. Takahashi, T. Okada, K. Nakano, Y. Ishida and A. Kameyama, *Polym. J.*, 2021, **53**, 1213–1222; (*e*) Z. Li, Z. Li, J. Hu, X. Feng, M. Zhang, G. Duan, R. Zhang and Y. Li, *ACS Macro Lett.*, 2021, **10**, 1563–1569; (*f*) N. Hasan, K. Busse, A. Ullah, H. Hussain and J. Kressler, *Langmuir*, 2021, **37**, 13399–13408; (*g*) J.-F. Yin, H. Xiao, P. Xu, J. Yang, Z. Fan, Y. Ke, X. Ouyang, G. X. Liu, T. L. Sun, L. Tang, S. Z. D. Cheng and P. Yin, *Angew. Chem., Int. Ed.*, 2021, **60**, 22212–22218.

7 Recent papers, see: (*a*) S. Samanta, S. Sarkar and N. K. Singha, *ACS Appl. Mater. Interfaces*, 2023, **15**, 24812–24826; (*b*) J. Yang, Y. Zhang, M. Hao, J. Zhi and X. Qian, *Polymer*, 2023, **268**, 125719; (*c*) Q. Liu, M. Ye, G. Yu and A. Han, *J. Appl. Polym. Sci.*, 2023, **140**, e53429; (*d*) X. Xu, J. D. Skelly and J. Song, *ACS Appl. Mater. Interfaces*, 2023, **15**, 2693–2704; (*e*) S. Ida, T. Hikida, A. Kawai, T. Matsuda, S. Suzuki, H. Imoto, K. Naka and S. Kanaoka, *Polym. Chem.*, 2023, **14**, 2771–2778; (*f*) K. A. Stewart, D. P. DeLellis, J. J. Lessard, J. F. Rynk and B. S. Sumerlin, *ACS Appl. Mater. Interfaces*, 2023, **15**, 25212–25223.

8 Recent papers, see: (*a*) J. Dong, L. Li, P. Qiu, Y. Pan, Y. Niu, L. Sun, Z. Pan, Y. Liu, L. Tan, X. Xu, C. Xu, G. Luo, Q. Wang and H. Wang, *Adv. Mater.*, 2023, **35**, 2211487; (*b*) Y. Shao, B. Hou, W. Li, X. Yan, X. Wang, Y. Xu, Q. Dong, W. Li, J. He and W.-B. Zhang, *Macromolecules*, 2023, **56**, 1562–1571; (*c*) X. Liu, L. Tang, Y. Chen, M. Fu, Z.-H. Guo, W. Tang and K. Yue, *Macromol. Rapid Commun.*, 2023, **44**, 2200292; (*d*) C. M. MacInnis, G. R. Younes and M. Marić, *J. Appl. Polym. Sci.*, 2022, **139**, e53225.

9 (*a*) J. F. Brown and L. H. Vogt, *J. Am. Chem. Soc.*, 1965, **87**, 4313–4317; (*b*) F. J. Feher, S. H. Phillips and J. W. Ziller, *Chem. Commun.*, 1997, **33**, 829–830; (*c*) F. J. Feher, *Chem. Commun.*, 1998, **34**, 399–400.

10 (*a*) Y. Sato, H. Imoto and K. Naka, *J. Polym. Sci.*, 2020, **58**, 1456–1462; (*b*) Y. Tomioka, R. Tanaka, T. T. Pham, S. Yusa, H. Imoto and K. Naka, *Polym. J.*, 2024, **56**, 653–660; (*c*) S. Tajbakhsh and M. Marić, *J. Polym. Sci.*, 2020, **58**, 2741–2754; (*d*) X.-H. Zheng, J.-F. Zhao, T.-P. Zhao, T. Yang, X.-K. Ren, C.-Y. Liu, S. Yang and E.-Q. Chen, *Macromolecules*, 2018, **51**, 4484–4493; (*e*) C.-G. Chae, Y.-G. Yu, H.-B. Seo, M.-J. Kim, M. Y. L. N. Kishore and J.-S. Lee, *Polym. Chem.*, 2018, **9**, 5179–5189.

11 (*a*) A. Igarashi, H. Imoto and K. Naka, *Polym. Chem.*, 2022, **13**, 1228–1235; (*b*) A. Igarashi, Y. Ueda, R. Katoh, H. Imoto and K. Naka, *J. Polym. Sci.*, 2021, **59**, 131–138; (*c*) T. Nakano, K. Okamoto, H. Imoto and K. Naka, *Polym. J.*, 2023, **55**, 193–201; (*d*) K. Okamoto, A. Igarashi, H. Imoto and K. Naka, *J. Polym. Sci.*, 2022, **60**, 214–220.

12 (*a*) Y. Yasumoto, T. Yamanaka, S. Sakurai, H. Imoto and K. Naka, *Polym. J.*, 2016, **48**, 281–287; (*b*) H. Araki and K. Naka, *Polym. J.*, 2012, **44**, 340–346; (*c*) R. Suzuki, L. Li, H. Imoto, H. Takagi, S. Sakurai and K. Naka, *Polym. J.*, 2022, **54**, 1179–1190.

13 (*a*) E. Ihara, *Polym. J.*, 2025, **57**, 1–23; (*b*) H. Shimomoto, *Polym. J.*, 2020, **52**, 269–277; (*c*) E. Ihara, Poly(substituted Methylene) Synthesis: Construction of C–C Main Chain from One Carbon Unit, in *Polymer Materials. Advances in Polymer Science*, ed. K. S. Lee and S. Kobayashi, Springer, 2010, vol. 231.

14 (*a*) F. Kato, A. Chandra, M. Tokita, H. Asano, H. Shimomoto, E. Ihara and T. Hayakawa, *ACS Macro Lett.*, 2018, **7**, 37–41; (*b*) H. Shimomoto, R. Hohsaki, D. Hiramatsu, T. Itoh and E. Ihara, *Macromolecules*, 2020, **53**, 6369–6379.

15 T. Toma, J. Shimokawa and T. Fukuyama, *Org. Lett.*, 2007, **9**, 3195–3197.

16 H. Shimomoto, H. Asano, T. Itoh and E. Ihara, *Polym. Chem.*, 2015, **6**, 4709–4714.

17 E. Ihara, M. Akazawa, T. Itoh, M. Fujii, K. Yamashita, K. Inoue, T. Itoh and H. Shimomoto, *Macromolecules*, 2012, **45**, 6869–6877.

18 (*a*) H. Shimomoto, J. Kawamata, H. Murakami, K. Yamashita, T. Itoh and E. Ihara, *Polym. Chem.*, 2017, **8**, 4030–4037; (*b*) H. Shimomoto, Y. Miyano, K. Kinoshita, T. Itoh and E. Ihara, *Polym. Chem.*, 2023, **14**, 1007–1018.

19 M. Milovanović, R. Bošković, T. Tošić, L. Katsikas and I. G. Popović, *Polym. Degrad. Stab.*, 2006, **91**, 3221–3229.